ISSN 0027-1314, Moscow University Chemistry Bulletin, 2021, Vol. 76, No. 6, pp. 407–416. © Allerton Press, Inc., 2021.

Role of the Protein Environment in Photoisomerization of Type I and Type II Rhodopsins: a Theoretical Perspective

P. A. Kusochek[a], V. V. Logvinov[a], and A. V. Bochenkova[a, *]

[a] *Department of Chemistry, Moscow State University, Moscow, 119991 Russia*

**e-mail: bochenkova@phys.chem.msu.ru*

Received September 24, 2021; revised September 27, 2021; accepted September 28, 2021

Abstract—Primary photoisomerization reactions of the retinal protonated Schiff base (RPSB) inside type I and type II rhodopsins are ultrafast and exhibit high quantum yields. Specific protein environments are thought to facilitate photoisomerization of RPSB; however, the detailed mechanisms of tuning the reaction timescales and specificity are far from being understood. Here, by using molecular dynamics simulations and large-scale XMCQDPT2-based QM/MM modeling, we gain insight into the role played by the protein environment in specific photoisomerization of RPSB from all-*trans* to 13-*cis* in microbial rhodopsin KR2 and from 11-*cis* to all-*trans* in bovine visual rhodopsin. By analyzing the calculated vibronic band shapes, we explore the early-time excited-state dynamics of RPSB in both types of rhodopsins. We show that the protein environment changes vibrational modes, which become excited following the S_0–S_1 transition, by pre-twisting the chromophore about a certain double bond in the ground electronic state. This reduces a barrier that hinders intramolecular rotation in the excited state, thus facilitating photoisomerization across the specific double bond. Moreover, pre-twisting of RPSB also provides conditions for initial in-phase excitation of the fundamental vibrational modes involved in the reaction coordinate, enabling vibrationally coherent barrierless excited-state decay in the photochemistry of vision.

Keywords: microbial rhodopsin KR2, bovine visual rhodopsin, photoisomerization, retinal, multiconfiguration quasi-degenerate perturbation theory, QM/MM, vibronic band shapes

DOI: 10.3103/S0027131421060110

INTRODUCTION

Eukaryota, *Archaea* and *Bacteria* use the photoreceptor proteins, rhodopsins, for a variety of biological functions. Rhodopsins are classified into two groups, animal and microbial rhodopsins. Type I or microbial rhodopsins perform several functions and include light-driven ion pumps, light-gated ion channels, and photosensory receptors. Type II or animal rhodopsins are the main drivers of vision [1].

The chromophores of microbial and animal rhodopsins are all-*trans* and 11-*cis* retinal, respectively, which are covalently attached to a lysine residue via a protonated Schiff base linkage (RPSB). The primary photochemical reaction is RPSB photoisomerization from all-*trans* to 13-*cis* in microbial rhodopsins and from 11-*cis* to all-*trans* in animal rhodopsins [2] (see Scheme 1).

Various factors affect vertical excitation energies of RPSB. One of the main factors are the length of the π-conjugated polyene chain and the protonation state of RPSB [3]. Most microbial and animal rhodopsins have absorption maxima in the range of 520–580 and 480–525 nm, respectively [4]. The difference in the absorption maxima of RPSB in various rhodopsins is also associated with the ability of the protein environment to tune the spectroscopic properties of the chromophore. The protein environment alters the spectral properties of RPSB through electrostatic and steric interactions with the chromophore, as revealed in a number of theoretical [5–11] and experimental studies [5, 12–17]. The sensitivity of RPSB to the electrostatic interactions is associated with a charge-transfer character of the first optically bright excited state. Upon absorption of a photon, the electron density shifts from the β-ionone ring to the nitrogen atom of RPSB [18]. In microbial and animal rhodopsins, the positively charged nitrogen atom of RPSB interacts with a negatively charged counterion, and this interaction leads to the stabilization of the ground electronic state of the chromophore and results in a blue shift of the absorption maximum [19, 20]. Negatively charged amino acid residues located near the β-ionone ring lead, on the contrary, to the stabilization of the excited electronic state and results in a red shift of the absorption maximum [20]. In addition to the electrostatic factors, the absorption spectra of RPSB in various rhodopsins are influenced by its conformation, which can become twisted due to steric hindrance imposed by the protein environment. In microbial rhodopsin

KR2 and bovine visual rhodopsin, RPSB is in the 6-*s*-*trans* [21] and 6-*s*-*cis* [22] conformations, respectively, while the 6-*s*-*cis* conformer is stable in solution [23]. The 6-*s*-*cis* conformation of RPSB leads to a partial disruption of the conjugation between the β-ionone ring and the retinal polyene chain. In microbial rhodopsins, the 6-*s*-*trans* conformation, on the contrary, does not break the conjugation of the β-ionone ring with the retinal polyene chain. The extended π-conjugation in microbial rhodopsins, therefore, results in a red shift of the absorption maximum compared to that of animal rhodopsins.

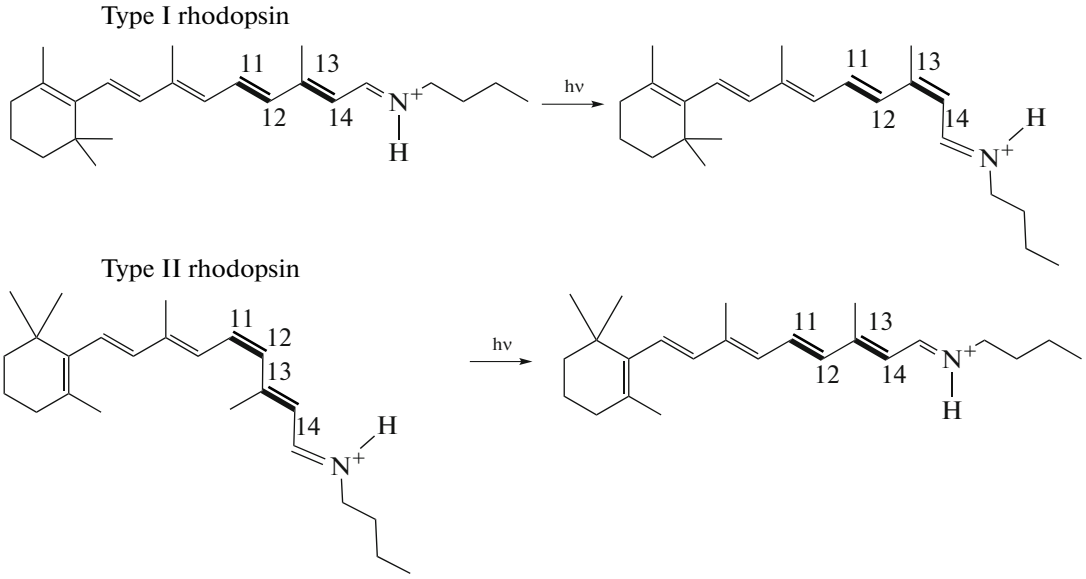

Scheme 1. Photoisomerization reactions of RPSB in type I and type II rhodopsins.

The primary photoisomerization reaction in rhodopsins is one of the fastest biological processes, which occurs on an ultrafast, sub-picosecond timescale with high quantum yields. The first discovered microbial bacteriorhodopsin serves as a proton pump in the archaeal membrane of *Halobacterium salinarum* and contains all-*trans* RPSB, which isomerizes upon photoexcitation from all-*trans* to 13-*cis* with high quantum yield (64%) and speed (500 fs) [24–26]. The first light-driven sodium-pump microbial rhodopsin KR2 from *Krokinobacter eikastus* has been discovered only recently [27]. It undergoes photoisomerization in 180 fs, which is almost three times faster than in bacteriorhodopsin. It is generally accepted that the interaction of RPSB with the protein environment accelerates photoisomerization, and this reaction takes about 2–10 ps in solution [25, 28, 29]. In solution, both 11-*cis* and 13-*cis* RPSB isomers are formed with quantum yields of 10–30% [25, 28, 30, 31].

Bovine visual rhodopsin (Rh) located in the membrane of light-sensitive rod cells is responsible for twilight vision in animals. It has an isomerization time of 200 fs [32–34] and a quantum yield of 65%. The 11-*cis* isomer of RPSB isomerizes much faster than the all-*trans* isomer in MeOH solution, but also exhibits a slow component with a characteristic timescale of 4 ps [35–37].

Photoisomerization of RPSB has also been considered in the gas phase, devoid of any external perturbations [38, 39]. The gas-phase studies are important as they provide a reference for studying the effect of different environments on the photophysical properties of RPSB, for example, on quantum yields and excited-state lifetimes. The reason for the lack of studies in this area is the complexity of the experiment, which requires very low concentrations of the chromophores in the gas phase, being an order of magnitude lower than those in solutions. The recent paper reports an experimental study of the photoisomerization dynamics of 11-*cis* and all-*trans* isomers of RPSB using time-resolved action absorption spectroscopy [40]. The experimental results have been supported by the high-level *ab initio* calculations at the XMCQDPT2/SA-CASSCF(12/12)/cc-pVDZ level of theory. It has been found that 11-*cis* RPSB undergoes almost barrierless isomerization, which occurs on a timescale of 400 fs, while all-*trans* RPSB shows barrier-controlled slow isomerization with a 3 ps time constant.

Therefore, both the all-*trans* and 11-*cis* RPSB chromophores show the sub-picosecond photoisomerization dynamics inside type I and type II rhodopsins, while their dynamics in solution is multi-exponential, with a slow picosecond component. At the same time, in the gas phase, the 11-*cis* isomer of RPSB exhibits the rate and selectivity of the photoisomerization reaction, which are comparable to those of 11-*cis* RPSB in visual rhodopsin. On the other hand, all-*trans* RPSB isomerizes by an order of magnitude

slower in the gas phase than in the protein environment, and photoisomerization proceeds across a different double bond in the polyene chain. Therefore, the protein environment unambiguously influences the dynamics of RPSB photoisomerization and enables the high speed and selectivity of this reaction in rhodopsins.

Several theoretical [41] and experimental [42, 43] studies have been devoted to the explanation of the influence of the protein environment on the RPSB photophysical properties. It has been established that point mutations of the negatively charged counterions of RPSB and the nearest charged amino acid residues located in the retinal-binding pocket to their neutral analogues slow down the photoisomerization reaction [42]. This effect is partly due to the fact that a number of charged amino acid residues maintain an ionized state of the RPSB counterion, which is important for the photoisomerization process. The impact of electron-donating and electron-withdrawing substituents introduced into the chemical structure of the chromophore in Dronpa2 on its photoisomerization barriers has been studied in detail [44]. It has been shown that the barriers are sensitive to such substitutions, since the excited state has a charge-transfer character that can be controlled by the external field. Steric hindrance and, in particular, pre-twisting of RPSB in the protein are also found to be important for ensuring high quantum yields and speed of the photoisomerization reaction [41, 43].

To date, a wide range of experimental and theoretical data has been accumulated, indicating the influence of the environment on the photophysical and photochemical properties of RPSB, which differ in the gas phase, solution, and proteins. It is mostly the protein environment that enables the high speed and specificity of the RPSB photoisomerization. Remarkably, type I and type II rhodopsins are striking examples of evolutionary convergence. They differ in many structural and mechanistic details and, most notably, they utilize different isomers of RPSB as their dark-adapted forms. However, type I and type II proteins from separate origins have been selected twice to be especially suited to photosensitive functions. To understand the role played by the proteins in specific photoisomerization of RPSB, it is important to compare the characteristics of this process in different environments. Here, by using high-level ab initio calculations, we compare the early-time photoinduced dynamics of RPSB in microbial rhodopsin KR2, bovine visual rhodopsin, and in isolated all-*trans* and 11-*cis* isomers.

METHODS

Molecular Dynamics

Full atomistic models of the KR2 protein and bovine visual rhodopsin in solution were obtained based on the X-ray structures with PDB ID 6REW [45] and PDB ID 1L9H [46], respectively. Coordinates of missing hydrogen atoms were added based on residue topologies. His residues were considered neutral with ε-nitrogen protonated. The structures were placed in a water box containing ~30000 water molecules. Geometry optimization of the solvated model systems was performed (2000 steps) followed by constant-temperature and constant-pressure NPT MD simulations with the CHARMM36 [47] force field parameters. The retinal parameters were obtained from Hayashi et al. [48, 49]. Water molecules were described with the TIP3P parameters [50]. Periodic boundary conditions were applied. The equilibration temperature was set to 300 K using the Langevin thermostat and the pressure was set to 1 atm using the Langevin piston Nosé–Hoover barostat. The particle mesh Ewald method was applied for treating long-range electrostatic interactions. The simulations were carried out with a 1 fs integration step for 40 ns. Then the temperature of the system was gradually lowered to 20 K in steps of 1 K during 1.06 ns. The final MD geometry was then obtained by performing energy minimization during another 10000 steps. The atomistic models of KR2 and bovine rhodopsin in aqueous solution were constructed using the VMD program [51]. The program NAMD was used to run MD simulations [52].

Ground-state QM/MM Calculations

The size of the MD annealed model systems was reduced for subsequent combined hybrid quantum mechanical/molecular mechanical (QM/MM) calculations. This was achieved by removing water molecules, which were farther than 2.4 Å from the protein surface. Each of the reduced systems contained about 480 water molecules, and the total number of atoms, including the protein, was ~5800. The RPSB chromophore together with the nearby amino acid residues constituted the QM part (see Fig. 1). The ground-state geometry optimization was performed within a mechanical embedding QM/MM scheme using ~1500 basis functions at the PBE0/(aug)-cc-pVDZ level of theory and modified AMBER [53] force field parameters. Diffuse functions were only affixed to the oxygen atoms. In the mechanical embedding QM/MM approach, restrictions were imposed on the geometry of the QM part, and interactions between the QM and MM parts were described using a classical MM force field. The current choice of the QM part correctly accounted for all interactions of the chromophore with the key residues, such as hydrogen bonding and short-range repulsion, treating the entire binding pocket at a sufficiently high level of theory. Additional constraints were imposed on the outer part of the protein, located more than 7 Å apart from the chromophore, which was kept fixed during the QM/MM optimization procedure.

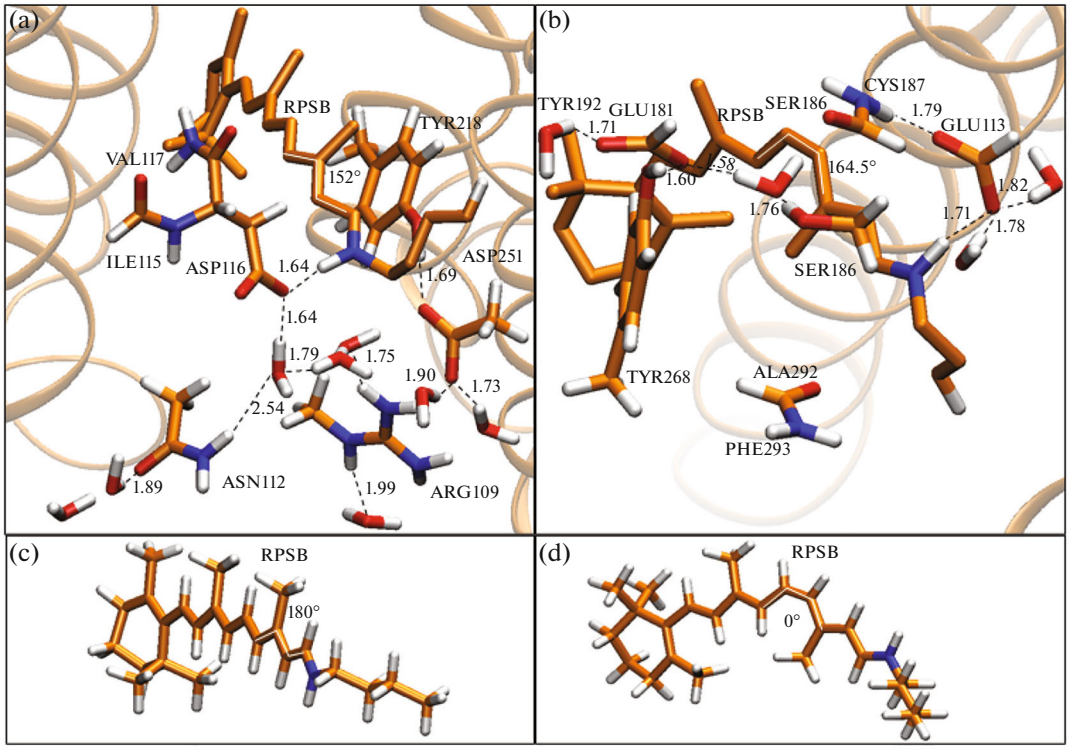

Fig. 1. Optimized structures of the active centers of KR2 rhodopsin derived from PDB ID 6REW (a), visual rhodopsin derived from PDB ID 1L9H (b) and isolated all-trans (c) and 11-*cis* (d) RPSB isomers. Highlighted with white are the torsion angles for rotation about the C_{13}–C_{14} bond (a, c) and the C_{11}–C_{12} bond (b, d). All distances are shown in Å.

Partial vibrational analysis was carried out within the framework of the same QM/MM approach, in which the second derivatives of the total QM/MM energy with respect to nuclear coordinates of RPSB and the side chain of Lys255 (in the case of KR2) or Lys296 (in the case of Rh) were calculated. The partially evaluated Hessian matrix was diagonalized, and its all positive eigenvalues (real frequencies) ensured that located QM/MM stationary points were true minima on the ground-state potential energy surface.

For all electronic structure calculations Firefly, version 8.2.0 [54], partially based on the GAMESS (US) source code [55], was used. The QM/MM functionality in Firefly is based on the integrated version of the Tinker Molecular Mechanics Package, version 3.7 [56].

Excited-state QM/MM Calculations

Vertical excitation energies were calculated in the optimized QM/MM structures, using the extended multiconfiguration quasi-degenerate perturbation theory (XMCQDPT2) [57] within the XMCQDPT2/SA-CASSCF(12,12)/(aug)-cc-pVDZ approach combined with the effective fragment potential (EFP) method [58] for treating the protein environment. The same QM parts were used for the excited-state QM/MM calculations. Only monopoles (partial point charges) of the MM part were included in the effective potentials, borrowed from the AMBER force field, i.e. the electrostatic embedding QM/MM scheme was applied. This method enabled polarization of the QM electron density in the field of the protein.

The reference wave functions of the ground state and the target excited states were constructed within the complete active space self-consistent field (CASSCF) method, with the active space (12,12) comprising 12 electrons distributed over 12 orbitals. All valence orbitals of the π-type were included in the active space. A state-averaging (SA) procedure was applied. Three lowest-lying CASSCF states were included in the SA procedure. The XMCQDPT2 effective Hamiltonians were constructed in the frame of the reference spaces spanned by 7 CASCI zero-order wavefunctions.

Excited-state gradient calculations were performed at the same level of theory, XMCQDPT2/SA(3)-CASSCF(12,12)/(aug)-cc-pVDZ. The effective Hamiltonians were constructed in the frame of the reference spaces spanned by three CASCI zero-order wave functions.

Simulations of Photoabsorption Profiles

The S_0–S_1 temperature-dependent Franck–Condon profiles of RPSB inside the protein environment

were calculated using the double harmonic parallel mode approximation based on direct evaluation of the overlap between vibrational wavefunctions in the S_0 and S_1 states. The origin shifts along normal modes of RPSB inside the protein environment (63 atoms and 183 normal modes) were calculated in the harmonic approximation based on the excited-state XMCQDPT2/CASSCF(12,12)/(aug)-cc-pVDZ//EFP gradient calculated at the Franck–Condon point. The final excited-state gradient was corrected by subtracting the ground-state gradient calculated at the same level of theory.

The original program (VibroniX) was used for calculating the photoabsorption profiles. The maximum vibrational excitation energy in S_1 was set to 10000 cm^{-1}. A maximum of 50 vibrational levels of each mode was considered in the ground electronic state occupied according to the Boltzmann distribution, and the level of excitation for each mode did not exceed 11. These parameters ensured that all relevant vibronic excitations were included, so that the sum of transition probabilities for each mode was equal to 1. The final spectral shapes were obtained by convoluting the calculated stick spectra with Gaussian functions. The method was previously applied for calculating vibronic band shapes of biological chromophores in various environments [59–61].

RESULTS AND DISCUSSION

Ground-state Structural and Vibrational Analysis

The structures of the QM/MM optimized active centers of the rhodopsins are shown in Fig. 1. In microbial rhodopsin KR2, the dihedral angle around the C_{13}–C_{14} bond (Fig. 1a) is 152°, and the dihedral angle around the C_{11}–C_{12} bond (Fig. 1b) is 164.5° in bovine visual rhodopsin. At the same time, the conformation of RPSB is planar in the gas phase (Figs. 1c, 1d). The deviation of these angles from planarity is partly due to the presence of a strong hydrogen bond between the protonated Schiff base of retinal and its counterpart, Asp116, in the case of rhodopsin KR2, and its counterion, Glu113, in the case of bovine visual rhodopsin.

The calculated harmonic frequencies of RPSB inside visual rhodopsin (Table 1), scaled with a coefficient of 0.953, are in good agreement with the previously calculated values [62] and with the experimental data on low-temperature Raman spectroscopy [63]. The calculated frequencies of RPSB inside rhodopsin KR2 also correlate well with the experimental data on IR [64], FTIR [65, 67], and Raman spectroscopy [68, 69] (Table 1). This supports the full atomistic models of KR2 and visual rhodopsin derived and used in the present study.

Analysis of the S_0–S_1 Photoabsroption Profiles

The calculated photoabsorption profiles of RPSB in the proteins are shown in Fig. 2. The Franck–Condon vibronic band shapes are calculated using the double harmonic parallel mode approximation with unscaled frequencies, neglecting anharmonicity of large amplitude soft modes, since these soft modes are inactive in the primary photoreaction. The calculated band shapes fully account for total widths of the experimental [70, 71] photoabsorption spectra. The major contribution to the width comes from high-frequency modes, in particular, from the active C=C stretch modes, while those with low frequencies promote spectral blurring.

The protein environment and the retinal conformation affect both the intensity and the number of high-frequency Franck–Condon active vibrational modes. In the KR2 rhodopsin, the C=C stretch mode, which is predominantly localized on the C_{13}–C_{14} bond with a frequency of 1609 cm^{-1}, is the most active upon the S_0–S_1 transition. In Fig. 2a, the peaks, which correspond to the 0–1 and 0–2 vibronic transitions of this mode, are indicated by numbers 2_0^1 and 2_0^2, respectively. The adiabatic 0–0 transition is denoted as 0_0^0. The stick spectrum of bovine visual rhodopsin looks similar to that of KR2 (Fig. 2b), but there is an important difference. In visual rhodopsin, the most active high-frequency Franck–Condon mode is the one localized on the C_{11}–C_{12} double bond with a frequency of 1636 cm^{-1}. The peaks, which correspond to the 0–1 and 0–2 vibronic transitions of this mode, are indicated by numbers 1_0^1 and 1_0^2, respectively.

Huang–Rhys factors, which are defined as squares of origin shifts in dimensionless normal coordinates divided by a factor of two, are useful in determining a relative activity of the modes upon photoabsorption. Figures 3a, 3b show the Huang–Rhys factors for microbial and visual rhodopsins, respectively. These spectra show that the hydrogen-out-of-plane (HOOP) modes also gain intensity inside both protein environments, whereas they are completely inactive for the all-*trans* and 11-*cis* isomers in the gas phase (Figs. 3c, 3d). The HOOP modes are associated with the H atom vibrations at the C_{14} atom in KR2 rhodopsin and with H atom vibrations at the C_{11} and C_{12} atoms in bovine visual rhodopsin.

The most active modes in these proteins are the high-frequency C=C stretch modes localized on the double bonds, which are mentioned above. The comparison of the Huang–Rhys factors of RPSB in the gas phase and inside the proteins shows that for both isomers in the gas phase, the Huang–Rhys factors of the stretching vibration along the C_{13}–C_{14} bond and along the C_{11}–C_{12} bond are nonzero; however, their overall intensity is lower by a factor of two. The protein environments selectively increase the intensity and the

Table 1. Experimental and calculated frequencies (cm^{-1}) of selected modes of RPSB in the retinal-binding pocket of KR2 rhodopsin and visual rhodopsin. Scaled frequencies with a factor of 0.953 are marked with an asterisk

Type I rhodopsin (KR2)			Type II rhodopsin (visual)		
assignment	experimental	calculated	assignment	experimental	calculated
C_{14} HOOP	877 [69]	905/862*	$C_{11}H{=}C_{12}H$ HOOP	970	1065/1015*
$C_{13}{=}C_{14}$ stretch	1532 [68], [69], [65], [64]	1609/1533*	$C_{10}{-}C_{11}$ stretch	1097	1133/1080*
N–D stretch	2095 [66], [67]	2084/1986*	$C_{14}{-}C_{15}$ stretch	1189	1265/1206*
$C_{10}{-}C_{11}$ stretch	1169 [66]	1210/1153*	$C_{11}{=}C_{12}$ stretch	1551	1636/1559*
$C_{14}{-}C_{15}$ stretch	1203 [66]	1243/1185*	C_{15}–NH stretch	1655	1746/1664*

corresponding Huang–Rhys factors for only one C=C stretch mode. In rhodopsin KR2, the most active mode becomes predominantly localized on the $C_{13}{-}C_{14}$ bond, whereas in bovine visual rhodopsin, this mode becomes predominantly localized on the $C_{11}{-}C_{12}$ bond.

By analyzing the vibronic band shapes of type I and type II rhodopsins, we get insight into the early-time photoinduced nuclear dynamics of RPSB in the excited state in different environments. Vibrational modes that become excited upon photoabsorption are remarkably different in KR2 and visual rhodopsin, although their overall vibrationally unresolved photoabsorption band shapes are alike. It has been shown theoretically [34, 73–75] and experimentally [34] that the corresponding C=C stretch and HOOP modes play a major role in the subsequent photoisomerization dynamics of RPSB, which occurs far beyond the Franck–Condon region. Here, we show that the protein environment facilitates specific photoisomerization of RPSB by initial excitation of the selected vibrational modes right after the vertical transition to the S_1 state in the Franck–Condon region. In this regard, type I and type II rhodopsins act in a similar fashion that ensures the efficiency of their photosensitive

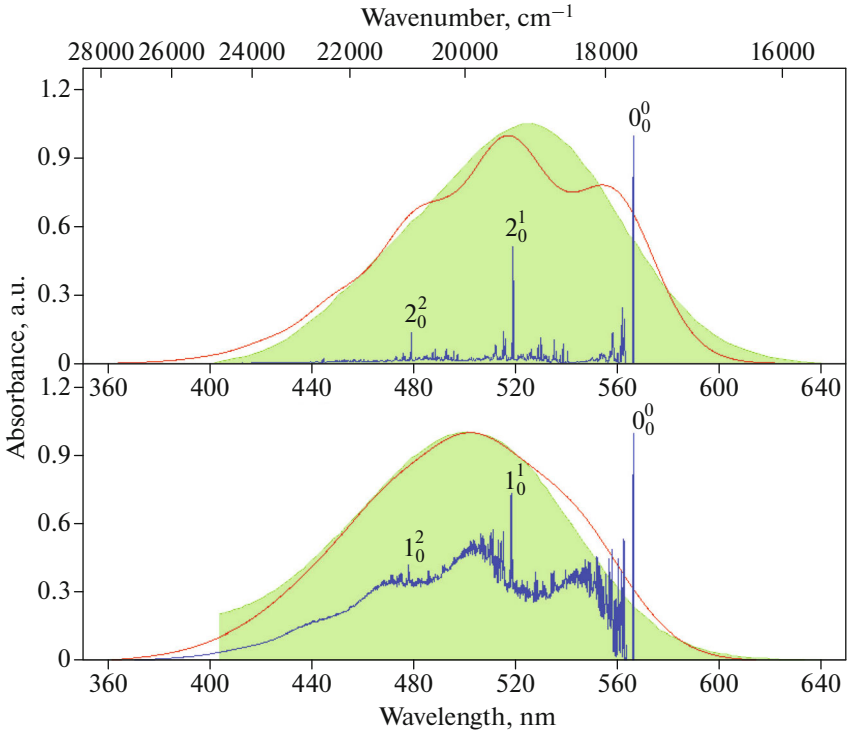

Fig. 2. Photoabsorption profiles of RPSB in KR2 rhodopsin (a) and visual rhodopsin (b) calculated at 300 K and convoluted with a Gaussian function with a half width at half maximum (HWHM) of 471 cm^{-1} (red line). The experimental spectra [70, 71] are shown in shaded green. Also presented are the stick spectra (blue line) calculated at 1 K and convoluted with a Gaussian function with a HWHM of 4 cm^{-1}. The numbers mark vibronic transitions for the most active C=C stretch modes predominantly localized on the $C_{11}{-}C_{12}$ (1) and $C_{13}{-}C_{14}$ (2) double bonds.

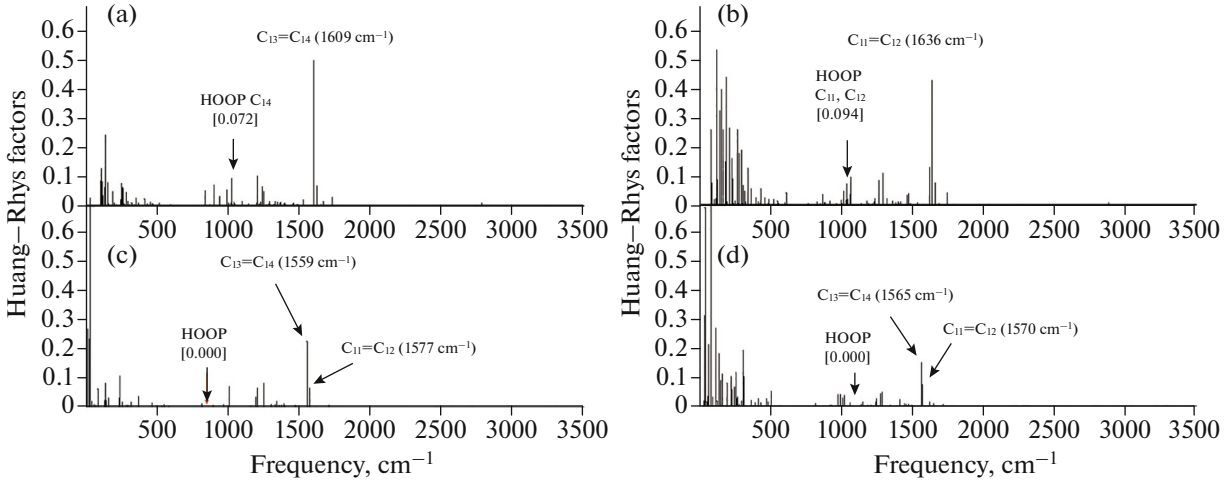

Fig. 3. Active Franck–Condon modes of RPSB upon the S_0–S_1 transition in KR2 rhodopsin (a), visual rhodopsin (b), and isolated all-trans (c) and 11-*cis* (d) isomers. Shown are the Huang–Rhys factors. Red arrows mark the HOOP modes with the corresponding Huang–Rhys factors indicated in square brackets. Note that the HOOP modes gain intensity in the protein environments.

function. The question then arises how the protein environment controls the selective excitation of those vibrational modes that are subsequently involved in the specific photoisomerization of RPSB.

It turns out that pre-twisting of RPSB about the specific double bond in the protein environment of KR2 and visual rhodopsin increases the intensity of the high-frequency stretching and HOOP vibrational modes localized on the twisted bond. These vibrations facilitate the subsequent specific photoisomerization reaction of RPSB from all-*trans* to 13-*cis* and from 11-*cis* to all-*trans* in KR2 and visual rhodopsin, respectively. We have previously shown that pre-twisting of RPSB has direct impact on vibrational modes that become active upon excitation in the structurally inhomogeneous protein KR2 [76]. The active site of KR2 can adapt various RPSB conformations stabilized by the nearest protein surrounding. Formation of a strong hydrogen bond between the retinal Schiff base and the RPSB primary counterion is found to be important for pre-twisting of RPSB in its most stable configuration, which, in turn, has impact on excitation of those vibrational modes that are involved in the photoisomerization reaction. Energetically less stable conformations exhibit less twisted conformations of RPSB, providing an explanation for the origin of non-reactive long-lived states in the excited-state decay of KR2.

Type II rhodopsins largely rely on the intrinsic properties of the isolated 11-*cis* RPSB chromophore, which shows ultrafast excited-state decay in the gas phase on a timescale of 400 fs [40]. This time is similar to that of the RPSB photoisomerization inside visual rhodopsin, where the primary ground-state photoproduct is formed in 200 fs [34]. The most recent study, however, reports that the first step in vision occurs exceedingly ultrafast in less than 50 fs, which is associated with a passage of a coherent vibrational wave packet through a conical intersection [77]. At the same time, type I rhodopsins change both the time scale and the specificity of the photoisomerization reaction as compared to those in the gas phase. All-*trans* RPSB decays in 3 ps in the gas phase at room temperature, which is accompanied by rotation about the C_{11}–C_{12} double bond [40], whereas the chromophore isomerizes from all-*trans* to 13-*cis* on a timescale of 180 fs in KR2 [27]. The markedly different timescales of the isolated all-*trans* and 11-*cis* isomers can be traced to the presence of a barrier that hinders rotation in the excited state of all-*trans* RPSB. Indeed, the excited-state barrier, which has been previously obtained at the XMCQDPT2 level of theory, is small (0.04 eV), yet non-negligible [40]. Therefore, the protein environment is likely to reduce the barrier heights through steric and electrostatic interactions with the chromophore in type I rhodopsins. Our results show that both type I and type II rhodopsins indeed change the conformation of RPSB, which becomes twisted about certain double bonds inside the protein environment, thus facilitating specific photoisomerization.

Importantly, we also reveal that by pre-twisting of RPSB, both types of the proteins alter the early-time photoinduced nuclear dynamics in the excited state, thus providing conditions for initial in-phase excitation of those vibrational modes that are involved in the photoisomerization. Indeed, the importance of intramolecular multimode vibrational coherence in the photochemistry of visual rhodopsin has been demonstrated recently [78], and the high quantum yield of the photoisomerization reaction is traced to the dynamic phase relationship achieved at the conical intersection by the modes involved in the reaction

coordinate. The vibrationally coherent and exceedingly ultrafast primary reaction in vision thus directly relies on the initial excitation conditions created by the protein environment.

CONCLUSIONS

By using the high-level extended multi-configuration quasi-degenerate perturbation theory combined with the effective fragment potential method, we calculate the photoabsorption spectral profiles of the RPSB chromophore inside the active centers of microbial rhodopsin KR2 and bovine visual rhodopsin and compare them to those calculated in the gas phase. The analysis of vibronic band shapes allows us to explore the early-time excited-state dynamics of RPSB in different environments and to show that it can significantly be altered by the specific protein environment. Pre-twisting of the chromophore about a specific double bond in the ground electronic state inside these proteins enhances the activity of both the localized C=C stretch and hydrogen-out-of-plane modes upon photoexcitation. These vibrational modes, which become excited in the S_1 state, facilitate the specific photoisomerization of RPSB from all-*trans* to 13-*cis* and from 11-*cis* to all-*trans* in microbial and animal rhodopsins, respectively. For the first time, our findings provide a direct link between the structure of the retinal-binding pocket and the early-time reaction dynamics of RPSB inside microbial and animal rhodopsins. We conclude that the role of the protein environment is not only in changing the structure of RPSB, which most certainly alters its excited-state potential energy surface through steric and electrostatic interactions of the protein environment with the chromophore, but also in providing conditions for initial in-phase excitation of the fundamental vibrational modes involved in the reaction coordinate.

ACKNOWLEDGMENTS

The calculations are carried out using the equipment of the shared research facilities of HPC computing resources at Lomonosov Moscow State University and the local resources provided through the Lomonosov Moscow State University Program of Development.

FUNDING

This work is supported by the Russian Foundation for Basic Research (grant no. 19-33-90254).

CONFLICT OF INTEREST

We have no conflicts of interest to disclose.

REFERENCES

1. Kandori, H., *Front. Mol. Biosci.*, 2015, vol. 2, 52.
2. Ernst, O.P., Lodowski, D.T., Elstner, M., Hegemann, P., Brown, L.S., and Kandori, H., *Chem. Rev.*, 2014, vol. 114, no. 1, p. 126.
3. Kakitani, H., Kakitani, T., Rodman, H., and Honig, B., *Photochem. Photobiol.*, 1985, vol. 41, no. 4, p. 471.
4. Oprian, D.D., Asenjo, A.B., Lee, N., and Pelletier, S.L., *Biochemistry*, 1991, vol. 30, no. 48, p. 11367.
5. Liu, R.S.H., Krogh, E., Li, X.-Y., Mead, D., Colmenares, L.U., Thiel, J.R., Ellis, J., Wong, D., and Asato, A.E., *Photochem. Photobiol.*, 1993, vol. 58, no. 5, p. 701.
6. Fujimoto, K., Hayashi, S., Hasegawa, J., and Nakatsuji, H., *J. Chem. Theory Comput.*, 2007, vol. 3, no. 2, p. 605.
7. Altun, A., Yokoyama, S., and Morokuma, K., *J. Phys. Chem. B*, 2008, vol. 112, no. 22, p. 6814.
8. Sekharan, S., Altun, A., and Morokuma, K., *J. Am. Chem. Soc.*, 2011, vol. 7, p. 215.
9. Melaccio, F., Ferré, N., and Olivucci, M., *Phys. Chem. Chem. Phys.*, 2012, vol. 14, no. 36, p. 12485.
10. Rangarajan, R., Galan, J.F., Whited, G., and Birge, R.R., *Biochemistry*, 2007, vol. 46, no. 44, p. 12679.
11. Sekharan, S., Sugihara, M., and Buss, V., *Angew. Chem., Int. Ed.*, 2007, vol. 46, nos. 1–2, p. 269.
12. Motto, M.G., Sheves, M., Tsujimoto, K., Balogh-Nair, V., and Nakanishi, K., *J. Am. Chem. Soc.*, 1980, vol. 102, no. 27, p. 7947.
13. Yan, B., Spudich, J.L., Mazur, P., Vunnam, S., Der guini, F., and Nakanishi, K., *J. Biol. Chem.*, 1995, vol. 270, no. 50, p. 29668.
14. Krebs, M.P., Mollaaghababa, R., and Khorana, H.G., *Proc. Natl. Acad. Sci. U. S. A.*, 1993, vol. 90, no. 5, p. 1987.
15. Wang, W., Nossoni, Z., Berbasova, T., Watson, C.T., Yapici, I., Lee, K.S.S., Vasileiou, C., Geiger, J.H., and Borhan, B., *Science*, 2012, vol. 338, no. 6112, p. 1340.
16. Cheng, C., Kamiya, M., Uchida, Y., and Hayashi, S., *J. Am. Chem. Soc.*, 2015, vol. 137, no. 41, p. 13362.
17. Kochendoerfer, G.G., Lin, S.W., Sakmar, T.P., and Mathies, R.A., *Trends Biochem. Sci.*, 1999, vol. 24, no. 8, p. 300.
18. Schenkl, S., *Science*, 2005, vol. 309, no. 5736, p. 917.
19. Blatz, P.E., Mohler, J.H., and Navangul, H.V., *Biochemistry*, 1972, vol. 11, no. 5, p. 848.
20. Andersen, L.H., Nielsen, I.B., Kristensen, M.B., El Ghazaly, M.O.A., Haacke, S., Nielsen, M.B., and Petersen, M.Å., *J. Am. Chem. Soc.*, 2005, vol. 127, no. 35, p. 12347.
21. Spudich, J.L., Yang, C.-S., Jung, K.-H., and Spudich, E.N., *Annu. Rev. Cell Dev. Biol.*, 2000, vol. 16, no. 1, p. 365.
22. Ahuja, S., Eilers, M., Hirshfeld, A., Yan, E.C.Y., Ziliox, M., Sakmar, T.P., Sheves, M., and Smith, S.O., *J. Am. Chem. Soc.*, 2009, vol. 131, no. 42, p. 15160.
23. Childs, R.F., Shaw, G.S., and Wasylishen, R.E., *J. Am. Chem. Soc.*, 1987, vol. 109, no. 18, p. 5362.
24. Mathies, R., Brito Cruz, C., Pollard, W., and Shank, C., *Science*, 1988, vol. 240, no. 4853, p. 777.
25. Hamm, P., Zurek, M., Röschinger, T., Patzelt, H., Oesterhelt, D., and Zinth, W., *Chem. Phys. Lett.*, 1996, vol. 263, no. 5, p. 613.

26. Logunov, S.L. and El-Sayed, M.A., *J. Phys. Chem. B*, 1997, vol. 101, no. 33, p. 6629.
27. Tahara, S., Takeuchi, S., Abe-Yoshizumi, R., Inoue, K., Ohtani, H., Kandori, H., and Tahara, T., *J. Phys. Chem. Lett.*, 2015, vol. 6, no. 22, p. 4481.
28. Logunov, S.L., Song, L., and El-Sayed, M.A., *J. Phys. Chem.*, 1996, vol. 100, no. 47, p. 18586.
29. Kandori, H. and Sasabe, H., *Chem. Phys. Lett.*, 1993, Vol. 216, nos. 1–2, p. 126.
30. Freedman, K.A., and Becker, R.S., *J. Am. Chem. Soc.*, 1986, vol. 108, no. 6, p. 1245.
31. Koyama, Y., Kubo, K., Komori, M., Yasuda, H., and Mukai, Y., *Photochem. Photobiol.*, 1991, vol. 54, no. 3, p. 433.
32. Schoenlein, R., Peteanu, L., Mathies, R., and Shank, C., *Science*, 1991, vol. 254, no. 5030, p. 412.
33. Peteanu, L.A., Schoenlein, R.W., Wang, Q., Mathies, R.A., and Shank, C. V., *Proc. Natl. Acad. Sci. U. S. A.*,1993, vol. 90, no. 24, p. 11762.
34. Polli, D., Altoè, P., Weingart, O., Spillane, K.M., Manzoni, C., Brida, D., Tomasello, G., Orlandi, G., Kukura, P., Mathies, R.A., Garavelli, M., and Cerullo, G., *Nature*, 2010, vol. 467, no. 7314, p. 440.
35. Becker, R.S. and Freedman, K., *J. Am. Chem. Soc.*, 1985, vol. 107, no. 6, p. 1477.
36. Kandori, H., Katsuta, Y., Ito, M., and Sasabe, H., *J. Am. Chem. Soc.*, 1995, vol. 117, no. 9, p. 2669.
37. Bassolino, G., Sovdat, T., Soares Duarte, A., Lim, J.M., Schnedermann, C., Liebel, M., Odell, B., Claridge, T.D.W., Fletcher, S.P., and Kukura, P., *J. Am. Chem. Soc.*, 2015, vol. 137, no. 39, p. 12434.
38. Toker, Y., Rahbek, D.B., Kiefer, H. V., Rajput, J., Antoine, R., Dugourd, P., Nielsen, S.B., Bochenkova, A.V., and Andersen, L.H., *Phys. Chem. Chem. Phys.*, 2013, vol. 15, no. 45, p. 19566.
39. Coughlan, N.J.A., Catani, K.J., Adamson, B.D., Wille, U., and Bieske, E.J., *J. Chem. Phys.*, 2014, vol. 140, no. 16, p. 164307.
40. Kiefer, H.V., Gruber, E., Langeland, J., Kusochek, P.A., Bochenkova, A.V., and Andersen, L.H., *Nat. Commun.*, 2019, vol. 10, no. 1, p. 1210.
41. Sugihara, M., Hufen, J., and Buss, V., *Biochemistry*, 2006, vol. 45, no. 3, p. 801.
42. Song, L., El-Sayed, M.A., and Lanyi, J.K., *Science*, 1993, vol. 261, no. 5123, p. 891.
43. Kochendoerfer, G.G., Verdegem, P.J.E., van der Hoef, I., Lugtenburg, J., and Mathies, R.A., *Biochemistry*, 1996, vol. 35, no. 50, p. 16230.
44. Romei, M.G., Lin, C.-Y., Mathews, I.I., and Boxer, S.G., *Science*, 2020, vol. 367, no. 6473, p. 76.
45. Kovalev, K., Polovinkin, V., Gushchin, I., Alekseev, A., Shevchenko, V., Borshchevskiy, V., Astashkin, R., Balandin, T., Bratanov, D., Vaganova, S., Popov, A., Chupin, V., Büldt, G., Bamberg, E., and Gordeliy, V., *Sci. Adv.*, 2019, vol. 5, no. 4, eaav2671.
46. Okada, T., Fujiyoshi, Y., Silow, M., Navarro, J., Landau, E.M., and Shichida, Y., *Proc. Natl. Acad. Sci. U. S. A.*, 2002, vol. 99, no. 9, p. 5982.
47. MacKerell, A.D., Jr., Bashford, D., Bellott, M., et al., *J. Phys. Chem. B*, 1998, vol. 102, no. 18, p. 3586.
48. Hayashi, S. and Ohmine, I., *J. Phys. Chem. B*, 2000, vol. 104, no. 45, p. 10678.
49. Hayashi, S., Tajkhorshid, E., Pebay-Peyroula, E., Royant, A., Landau, E.M., Navarro, J., and Schulten, K., *J. Phys. Chem. B*, 2001, vol. 105, no. 41, p. 10124.
50. Jorgensen, W.L., Chandrasekhar, J., Madura, J.D., Impey, R.W., and Klein, M.L., *J. Chem. Phys.*, 1983, vol. 79, no. 2, p. 926.
51. Humphrey, W., Dalke, A., and Schulten, K., *J. Mol. Graphics*, 1996, vol. 14, no. 1, p. 33.
52. Phillips, J.C., Braun, R., Wang, W., Gumbart, J., Tajkhorshid, E., Villa, E., Chipot, C., Skeel, R.D., Kalé, L., and Schulten, K., *J. Comput. Chem.*, 2005, vol. 26, no. 16, p. 1781.
53. Cornell, W.D., Cieplak, P., Bayly, C.I., Gould, I.R., Merz, K.M., Ferguson, D.M., Spellmeyer, D.C., Fox, T., Caldwell, J.W., and Kollman, P.A., *J. Am. Chem. Soc.*, 1995, vol. 117, no. 19, p. 5179.
54. Granovsky, A.A. Firefly version 8. http://classic.chem.msu.su/gran/firefly/index.html.
55. Schmidt, M.W., Baldridge, K.K., Boatz, J.A., Elbert, S.T., Gordon, M.S., Jensen, J.H., Koseki, S., Matsunaga, N., Nguyen, K.A., Su, S., Windus, T.L., Dupuis, M., and Montgomery, J.A., *J. Comput. Chem.*, 1993, vol. 14, no. 11, p. 1347.
56. Rackers, J.A., Wang, Z., Lu, C., Laury, M.L., Lagardère, L., Schnieders, M.J., Piquemal, J.-P., Ren, P., and Ponder, J.W., *J. Chem. Theory Comput.* 2018, vol. 14, no. 10, p. 5273.
57. Granovsky, A.A., *J. Chem. Phys.*, 2011, vol. 134, no. 21, 214113.
58. Day, P.N., Jensen, J.H., Gordon, M.S., Webb, S.P., Stevens, W.J., Krauss, M., Garmer, D., Basch, H., and Cohen, D., *J. Chem. Phys.*, 1996, vol. 105, no. 5, p. 1968.
59. Kiefer, H.V., Lattouf, E., Persen, N.W., Bochenkova, A.V., and Andersen, L.H., *Phys. Chem. Chem. Phys.*, 2015, vol. 17, no. 31, p. 20056.
60. Bochenkova, A.V. and Andersen, L.H., *Faraday Discuss.*, 2013, vol. 163, p. 297.
61. Bochenkova, A.V. and Andersen, L.H., in *Photophysics of Ionic Biochromophores*, Berlin: Springer, 2013, p. 67.
62. Khrenova, M.G., Bochenkova, A.V., and Nemukhin, A.V., *Proteins: Struct., Funct., Bioinf.*, 2010, vol. 78, no. 3, p. 614.
63. Lin, S.W., Groesbeek, M., van der Hoef, I., Verdegem, P., Lugtenburg, J., and Mathies, R.A., *J. Phys. Chem. B*, 1998, vol. 102, no. 15, p. 2787.
64. Asido, M., Eberhardt, P., Kriebel, C.N., Braun, M., Glaubitz, C., and Wachtveitl, J., *Phys. Chem. Chem. Phys.*, 2019, vol. 21, no. 8, p. 4461.
65. Chen, H.-F., Inoue, K., Ono, H., Abe-Yoshizumi, R., Wada, A., and Kandori, H., *Phys. Chem. Chem. Phys.*, 2018, vol. 20, no. 26, p. 17694.
66. Ono, H., Inoue, K., Abe-Yoshizumi, R., and Kandori, H., *J. Phys. Chem. B*, 2014, vol. 118, no. 18, p. 4784.
67. Tomida, S., Ito, S., Mato, T., Furutani, Y., Inoue, K., and Kandori, H., *Biochim. Biophys. Acta, Bioenerg.*, 2020, vol. 1861, no. 7, 148190.

68. Hontani, Y., Inoue, K., Kloz, M., Kato, Y., Kandori, H., and Kennis, J.T.M., *Phys. Chem. Chem. Phys.*, 2016, vol. 18, no. 35, p. 24729.

69. Nishimura, N., Mizuno, M., Kandori, H., and Mizutani, Y., *J. Phys. Chem. B*, 2019, vol. 123, no. 16, p. 3430.

70. Inoue, K., Ono, H., Abe-Yoshizumi, R., Yoshizawa, S., Ito, H., Kogure, K., and Kandori, H., *Nat. Commun.*, 2013, vol. 4, no. 1, p. 1678.

71. Kandori, H., Shichida, Y., and Yoshizawa, T., *Biochemistry*, 2001, vol. 66, p. 1197.

72. Schapiro, I., Ryazantsev, M.N., Frutos, L.M., Ferré, N., Lindh, R., and Olivucci, M., *J. Am. Chem. Soc.*, 2011, vol. 133, no. 10, p. 3354.

73. Hayashi, S., Tajkhorshid, E., and Schulten, K., *Biophys. J.*, 2009, vol. 96, no. 2, p. 403.

74. Coto, P.B., Sinicropi, A., De Vico, L., Ferré, N., and Olivucci, M., *Mol. Phys.*, 2006, vol. 104, nos. 5–7, p. 983.

75. Gozem, S., Luk, H.L., Schapiro, I., and Olivucci, M., *Chem. Rev.*, 2017, vol. 117, no. 22, p. 13502.

76. Kusochek, P.A., Scherbinin, A.V., and Bochenkova, A.V., *J. Phys. Chem. Lett.*, 2021, vol. 12, no. 35, p. 8664.

77. Johnson, P.J.M., Halpin, A., Morizumi, T., Prokhorenko, V.I., Ernst, O.P., and Miller, R.J.D., *Nat. Chem.*, 2015, vol. 7, no. 12, p. 980.

78. Schnedermann, C., Yang, X., Liebel, M., Spillane, K.M., Lugtenburg, J., Fernández, I., Valentini, A., Schapiro, I., Olivucci, M., Kukura, P., and Mathies, R.A., *Nat. Chem.*, 2018, vol. 10, no. 4, p. 449.